Photonic interaction between quantum dots and gold nanoparticles in discrete nanostructures through DNA directed self-assembly†

Qiangbin Wang,*[a] Haining Wang,[b] Chenxiang Lin,[cd] Jaswinder Sharma,[cd] Shengli Zou*[b] and Yan Liu*[cd]

Received (in Cambridge, UK) 31st July 2009, Accepted 3rd November 2009
First published as an Advance Article on the web 18th November 2009
DOI: 10.1039/b915712c

Discrete nanostructures of CdSe@ZnS QDs and Au NPs were prepared and the photonic interactions between the QDs and Au NPs were systematically investigated. We found that the Au/QD ratio, separation distances between Au NPs and QDs, and the size of the Au NPs in a given discrete nanostructure all affect the interaction between Au NPs and QDs.

The rational design and assembly of colloidal nanocrystals, such as Au, Ag nanoparticles (NPs), and quantum dots (QDs), *etc*., have attracted much attention in the past decades due to their novel optoelectrical properties.[1–5] Previous studies have shown that interactions with surface plasmons (SPs) can significantly affect the photoluminescence (PL) intensities of QDs, in which the QD PL intensity is either enhanced or diminished by the proximal metal NPs due to the competition between field enhancement and nonradiative energy transfer to SPs.[6–8] Nevertheless, investigations aimed at probing the nature of the interactions between luminescent QDs and Au NPs embedded in controlled assemblies, and how those interactions could affect the optical properties of these assemblies, remain rather limited.[9] In particular, it has been an attractive goal to study such properties with control of the distance between the Au NPs and QDs and also the Au/QD ratio.

DNA nanotechnology has created unique opportunities to generate functional, multicomponent nanoarchitectures.[10–15] With DNA as excellent templates, spatially positioning nanoparticles with sub-nanometre precision and programmability has been accomplished.[16] Herein, we report the photonic interactions between QDs and Au NPs in discrete nanostructures by grouping CdSe@ZnS QDs with Au NPs through DNA self-assembly. Specifically, the nanostructures with one QD in the center and a discrete number of Au NPs attached, are generated through hybridization of complementary DNA bound to the QD and Au NPs, as illustrated in Scheme 1. In this study, 5 nm and 10 nm Au NPs were used to construct the Au–QD complexes, and 20mer (6.5 nm), 51mer (16.5 nm) and 114mer (37 nm) DNA sequences were utilized to tune the distances between the Au NPs and QDs.

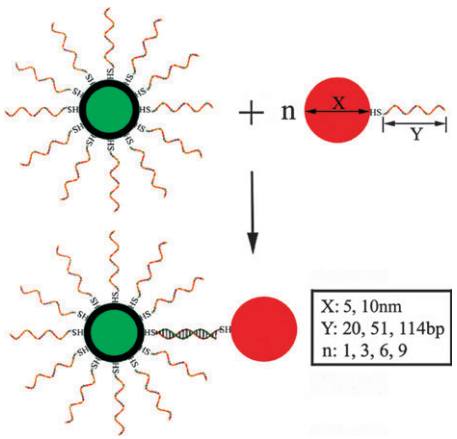

Scheme 1 Construction of QD–Au discrete nanostructures with controllable distance between Au and the QD (6.5, 16.5, 37 nm), size of Au NP (5, 10 nm) and Au/QD ratio (1, 3, 6, 9) through DNA directed self-assembly.

Adopting the established method,[14b] Au nanocrystals conjugated to one single strand of DNA were prepared and purified using gel electrophoresis. To obtain the proposed QD–Au discrete nanostructures, it is critical to utilize Au NPs containing only one ssDNA on the surface, so that no cross-linking among particles happens in subsequent synthesis steps, therefore ensuring the formation of the designed nanostructures. Due to limitations of gel electrophoresis, the shortest length of DNA strand that can be employed to obtain 1 : 1 Au–DNA conjugates for 10 nm Au is a 90mer. Therefore, to prepare Au–51mer and Au–20mer single conjugates, a 90mer DNA strand is first used to obtain the 1 : 1 Au–DNA conjugate and then restriction digested in the presence of proper helper strands (DNA sequences and restriction digest details see ESI†).

The CdSe@ZnS core/shell QDs functionalized with DNA on the surface were prepared employing our recently developed *in situ* functionalization method.[17] In brief, the thiolated ssDNA was added directly as a ligand into the reaction during CdSe@ZnS QD formation. We simultaneously obtained CdSe@ZnS core/shell QDs as well as DNA functionality. Green emission QDs with an emission peak at 520 nm were applied in this study. Three different lengths of DNA, which were complementary to the DNA sequences conjugated on the Au NP surfaces, were directly conjugated onto the QD surfaces (DNA sequences see ESI†). To form the Au–QD nanostructures, the Au NPs conjugated with various lengths

[a] *Suzhou Institute of Nano Tech and Nano Bionics, Chinese Academy of Sciences, Suzhou 215125, China. E-mail: qbwang2008@sinano.ac.cn; Fax: +86-512-62872620; Tel: +86-512-62872620*
[b] *Department of Chemistry, University of Central Florida, Orlando, FL 32826, USA. E-mail: szou@mail.ucf.edu*
[c] *Department of Chemistry & Biochemistry, Arizona State University, Tempe, AZ 85287, USA*
[d] *The Biodesign Institute, Arizona State University, Tempe, AZ 85287, USA. E-mail: yan_liu@asu.edu*
† Electronic supplementary information (ESI) available: DNA sequences and restriction digest details. See DOI: 10.1039/b915712c

of DNA strands were mixed with QDs functionalized with the corresponding complementary strand in 1 × TBE buffer containing 500 mM NaCl at different QD/Au ratios (1 : 1, 1 : 3, 1 : 6 and 1 : 9). The mixture was heated at 90 °C for 5 min and then was slowly cooled to room temperature.

Transmission electron microscopy (TEM) observations were carried out on a JOEL 2010 FX operating at an accelerating voltage of 200 kV. Photoluminescence spectra of the above Au–QD nanostructures were recorded using a PTI spectrofluorometer. Lifetimes of QDs in different nanostructures were measured using the femtosecond transient spectroscopy system and decay-associated spectra (DAS) were calculated from global fitting accounting for deconvolution of the recorded signals with the instrument response function using locally written software (ASUFIT, web address: www.public.asu.edu/~laserweb/asufit/asufit.html).

Representative TEM images of the as-prepared discrete nanostructures are shown in Fig. 1. Fig. 1(a) to (d) show the nanostructures with different Au/QD ratios at a distance of 16.5 nm. Due to the drying process during sampling, the Au NPs aggregated as shown in Fig. 1(c) and (d), in which the QD could not be observed. Fig. 1(e)–(g) present the 3 : 1 Au–QD discrete nanostructures with different separation distances between Au NPs and the QD. The distances between the QD and Au NPs are measured to be around 5 nm, 14 nm and 27 nm from the TEM images, which are slightly smaller than the theoretical distances of 6.5 nm, 16.5 nm and 37 nm due to the drying on the TEM grid and the vacuum environment during TEM imaging. The QDs have a lower contrast than the Au NPs and are marked with white arrows in the TEM images. Note: TEM images may not represent the exact 3D geometry structure of the Au–QD assembly as TEM samples were imaged on a 2D grid and dried. The statistical analysis on several hundred Au nanoparticles shows that the yields of designed structures are around 65%.

The effects of the distance between QDs and Au NPs (~6.5 nm; ~16.5 nm; ~37 nm), the size of the Au NPs (5 nm; 10 nm), and the Au/QD ratio (1, 3, 6, 9) on the optical properties of the QDs were systematically investigated experimentally and compared with theoretical simulation results.

Steady-state PL was measured for each set of the above QD–DNA–Au structures. These data were further complemented with time-resolved fluorescence measurements

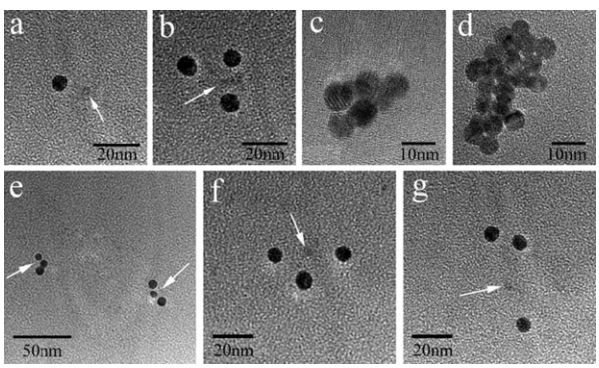

Fig. 1 Representative TEM images of different ratios of 10 nm Au NPs with QDs at a 51mer distance (a) 1 : 1, (b) 1 : 3, (c) 1 : 6, (d) 1 : 9 and then assembly of three Au NPs per QD with different DNA lengths (e) 20mer, (f) 51mer and (g) 114mer.

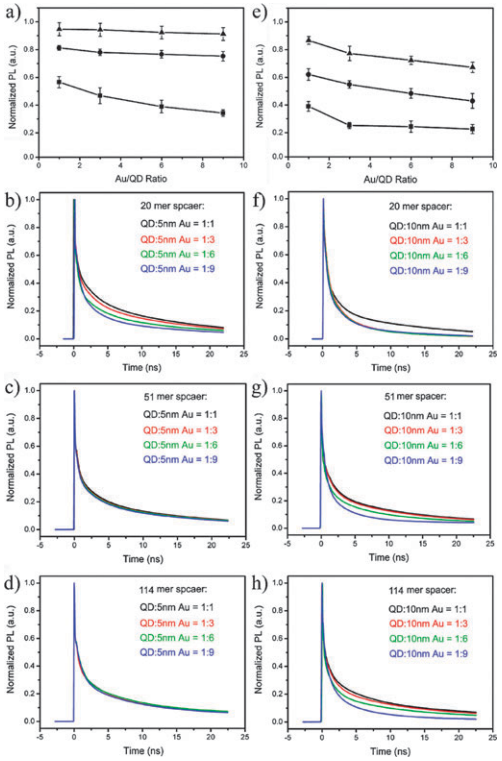

Fig. 2 (a) and (e) PL intensity of QDs in the different discrete nanostructures constructed from QDs surrounded with 5 and 10 nm Au NPs, respectively. The distances between Au and the QDs are ■: 6.5 nm; ●: 16.5 nm; ▲: 37 nm. (b–d and f–h) Time-resolved fluorescence measurements of QDs in the different nanostructures with different spacings between QDs and 5 and 10 nm Au NPs, respectively.

(Fig. 2). The Au NPs may absorb both the incident light and the emitted light from the QDs. This attenuation effect has been corrected by using samples with the same ratio of Au NPs and QDs but without DNA linkers as the normalization references so that only the quenching effect of the Au NPs directly linked to the quantum dots is considered. In fact, neither the adsorption of DNA nor the conjugated QDs affects the plasmonic characteristics of Au NPs.

For the structures containing 5 nm Au NPs (Fig. 2a), when the distance between Au and the QDs was about 6.5 nm, the PL quenching of the QDs was proportional to the Au/QD ratio. However, when the distances between the Au and the QDs were increased to 16.5 nm and 37 nm, the quenching of the Au NPs on QD PL is only 20% and ~8%, respectively, showing little dependence on the Au/QD ratios. Consistent with the PL intensity quenching results, we observed that the lifetimes of QDs in the discrete nanostructures decrease with increasing numbers of Au NPs at a distance of 6.5 nm (Fig. 2b–d). When the distance was increased to 16.5 nm and 37 nm, the lifetimes of the QDs remained constant when the Au/QD ratio was changed from 1 to 9. These results imply that the photonic interactions between the 5 nm Au NPs and the QDs are confined within a short distance. When the distance was increased, little interaction was observed in this system, possibly due to the weak energy transfer efficiency of the small sized Au NPs.

We further studied the photonic interaction between Au NPs and QDs with 10 nm Au NPs (Fig. 2e). For all the

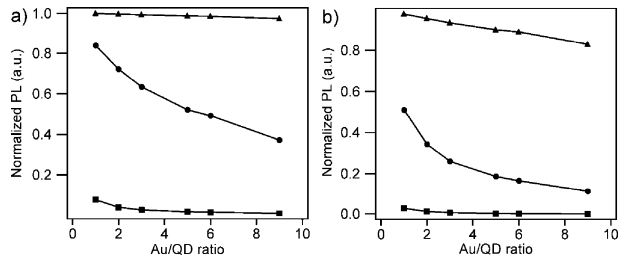

Fig. 3 Quenching ratio calculated using the modified coupled dipole method for (a) 5 nm and (b) 10 nm Au particles with different QD–Au distances: ■: 20mer spacer; ●: 51mer spacer; ▲: 114mer spacer at different Au/QD ratios.

structures created with the same Au/QD ratio and the same Au–QD distance, the quenching effect of the 10 nm Au NPs on the QD PL is much stronger than that of the 5 nm Au NPs. For example, at a distance of 6.5 nm, for the 1 : 1 Au–QD structure, with 10 nm Au NPs, the PL of the QDs dropped to 40% of the reference, which is lower than that with 5 nm Au NPs, which is ~60% of the reference. The PL intensity drops further with increasing Au/QD ratio. When the distance between the QDs and Au was increased to 16.5 nm and 37 nm, respectively, the quenching of the PL of the QDs is mitigated compared to the samples of shorter Au–QD distance, and both display a decreasing trend with Au/QD ratio. This is different from that with 5 nm Au NPs. The lifetime measurement data are consistent with and support the trends of steady-state PL quenching results (Fig. 2f–h). These results indicate that the larger sized Au NPs can have energy transfer with the QDs at relatively longer distances.

To further understand the mechanism behind the experimental observations, we calculated the PL intensity of QDs at different configurations using a modified coupled dipole method.[18] For a QD attached to several Au NPs, the PL signal can be amplified by the enhanced local electric field at the incident and emission wavelengths, the signal can also be quenched through non-radiative decay of the QD by the proximal Au NPs. The PL intensity of a QD with several Au NPs relative to that of a free QD can be calculated by equation:

$$f = f_{\text{inc}} \times f_{\text{emission}} \times q_{\text{emission}}, \quad (1)$$

where f is the PL intensity, f_{inc} and f_{emission} are the enhancement factors of the PL signal at the incident and emission wavelengths and q_{emission} represents the quenching factor of the PL signal by the surrounding Au NPs at the emission wavelength. In our calculations, f_{inc} and f_{emission} are proportional to the local electric field at the location of the QD, $|E|^2$, due to the surface plasmon excitation of the Au NPs at the incident and emission wavelengths. The enhanced local electric field can be calculated using Mie theory[19] and is averaged over different orientations. q_{emission} can be obtained by dividing the scattering cross-section of the QD surrounded by several Au NPs with that of the free QD at the emission wavelength. Note that only the QD is illuminated when calculating the scattering cross-section of the QD surrounded by several AuNPs and the cross-section is calculated by integrating the scattered light around the QD over a small sphere with no Au NPs included in the sphere. Fig. 3 shows the simulated results which exhibit qualitatively the same trend as the experimental data shown in Fig. 2a and e. The discrepancy between the experimental results and the calculated results may be attributed to the non-complete construction of Au–QD discrete nanostructures in the system.

In summary, we studied the photonic interactions between CdSe@ZnS QDs and Au NPs in discrete nanostructures through DNA directed self-assembly. By taking advantage of the robustness and addressability of DNA nanotechnology, we were able to achieve three unique features: (1) varying the Au/QD ratio in a given nanostructure, (2) tuning the separation distances between Au NPs and QDs in a broad range, and (3) changing the size of Au NPs in the discrete nanostructures. We found that all these factors affect the interaction between the Au NPs and QDs. The insights gained from the experimental results and theoretical simulations presented here may provide better understanding of the physical interactions between QDs and Au NPs, which are crucial to potential photonic applications of nanoparticle based research.

Q.W. is grateful for the financial support of the CAS/SAFEA International Partnership Program for Creative Research Teams. Y.L. thanks the NSF, ONR and NIH for funding. S.Z. thanks the ACS/PRF and NSF for support. The authors thank Dr Su Lin for help in using the laser facility.

Notes and references

1 A. P. Alivisatos, *Nat. Biotechnol.*, 2004, **22**, 47.
2 C. J. Murphy, *Anal. Chem.*, 2002, **74**, 520 A.
3 R. Elghanian, J. J. Storhoff, R. C. Mucic, R. L. Letsinger and C. A. Mirkin, *Science*, 1997, **277**, 1078.
4 S. Bidault, F. J. García de Abajo and A. Polman, *J. Am. Chem. Soc.*, 2008, **130**, 2750.
5 X. Wang, L. Liu, O. Ramstrom and M. Yan, *Exp. Biol. Med.*, 2009, **234**, 1128.
6 N. Liu, B. S. Prall and V. I. Klimov, *J. Am. Chem. Soc.*, 2006, **128**, 15362.
7 K. T. Shimizu, W. K. Woo, B. R. Fisher, H. J. Eisler and M. G. Bawendi, *Phys. Rev. Lett.*, 2002, **89**, 117401.
8 J. Lee, A. O. Govorov, J. Dulka and N. A. Kotov, *Nano Lett.*, 2004, **4**, 2323.
9 T. Pons, I. L. Medintz, K. E. Sapsford, S. Higashiya, A. F. Grimes, D. S. English and H. Mattoussi, *Nano Lett.*, 2007, **7**, 3157.
10 F. A. Aldaye, A. L. Palmer and H. F. Sleiman, *Science*, 2008, **321**, 1795.
11 C. Lin, Y. Liu and H. Yan, *Biochemistry*, 2009, **48**, 1663.
12 A. J. Mastroianni, S. A. Claridge and A. P. Alivisatos, *J. Am. Chem. Soc.*, 2009, **131**, 8455.
13 H. Meng, Y. Yang, Y. Chen, Y. Zhou, Y. Liu, X. Chen, H. Ma, Z. Tang, D. Liu and L. Jiang, *Chem. Commun.*, 2009, 2293.
14 (*a*) A. P. Alivisatos, K. P. Johnsson, X. Peng, T. E. Wilson, C. J. Loweth, M. P. Bruchez and P. G. Schultz, *Nature*, 1996, **382**, 609; (*b*) D. Zanchet, C. M. Micheel, W. J. Parak, D. Gerion, S. C. Williams and A. P. Alivisatos, *J. Phys. Chem. B*, 2002, **106**, 11758; (*c*) A. Fu, C. M. Micheel, J. Cha, H. Chang, H. Yang and A. P. Alivisatos, *J. Am. Chem. Soc.*, 2004, **126**, 10832.
15 (*a*) C. A. Mirkin, R. L. Letsinger, R. C. Mucic and J. J. Storhoff, *Nature*, 1996, **382**, 607; (*b*) N. L. Rosi and C. A. Mirkin, *Chem. Rev.*, 2005, **105**, 1547; (*c*) N. L. Rosi, D. A. Giljohann, C. S. Thaxton, A. K. R. Lytton-Jean, M. S. Han and C. A. Mirkin, *Science*, 2006, **312**, 1027.
16 (*a*) J. D. Le, Y. Pinto, N. C. Seeman, K. Musier-Forsyth, T. A. Taton and R. A. Kiehl, *Nano Lett.*, 2004, **4**, 2343; (*b*) F. A. Aldaye and H. F. Sleiman, *Angew. Chem., Int. Ed.*, 2006, **45**, 2204; (*c*) J. Bath and A. J. Turberfield, *Nat. Nanotechnol.*, 2007, **2**, 275; (*d*) N. C. Seeman, *Trends Biochem. Sci.*, 2005, **30**, 119.
17 Q. B. Wang, Y. Liu, Y. G. Ke and H. Yan, *Angew. Chem., Int. Ed.*, 2008, **47**, 316.
18 S. L. Zou and G. C. Schatz, *Phys. Rev. B*, 2006, **74**, 125111.
19 G. Mie, *Ann. Phys.*, 1908, **330**, 377.

